Supplemental Material

for

Functional Roles of Acetylated Histone Marks at Mouse Meiotic Recombination Hotspots

Irina V. Getun,[a,§,*] Zhen Wu,[a] Mohammad Fallahi,[b] Souad Ouizem,[c] Qin Liu,[c,¶] Weimin Li,[a,d] Roberta Costi,[e] William R. Roush,[c] John L. Cleveland,[a,d,*] Philippe R. J. Bois[a,§§]

[a]Department of Cancer Biology, The Scripps Research Institute, Jupiter, Florida, USA; [b]Informatics Core, The Scripps Research Institute, Jupiter, Florida, USA; [c]Department of Chemistry, The Scripps Research Institute, Jupiter, Florida, USA; [d]Department of Tumor Biology, H. Lee Moffitt Cancer Center and Research Institute, Florida, USA; [e]Dipartimento di Chimica e Tecnologie del Farmaco, Istituto Pasteur-Fondazione Cenci Bolognetti, "Sapienza" Università di Roma, Roma, Italy

Running Head: Histone Acetylation Controls Meiotic Hotspot Activity

*Address correspondence to Irina V. Getun, igetun@uthsc.edu or John L. Cleveland, John.Cleveland@moffitt.org.

[§]Present address: Department of Surgery, University of Tennessee Health Science Center, Memphis, Tennessee, USA.
[¶]Present address: School of Pure and Applied Science, Florida Southwestern State College, Fort Myers, Florida, USA.
[§§]Present address: Avespa, Miami, Florida, USA.

This PDF file includes:

SUPPLEMENTAL DATASETS

Dataset S1 Summary (provided as an Excel file):

A list of differentially expressed genes encoding HAT, HDAC, HMT and HDMT enzymes is provided (*p*-value [corrected] <0.05), and these are sorted by $\log_2$ fold change of spermatogonia/average pachytene expression ($\log_2$ ratio ≥0.58 and ≤-0.58). Heatmaps of differentially expressed genes encoding histone-modifying enzymes are shown in Figs. 1, Fig. S6A and C and Fig. S7A and C. A full list of genes encoding histone modification enzymes and their $\log_2$ median normalized expression values in *Spo11*$^{-/-}$ and wild-type (WT) meiotic cell stages are also provided. HAT, HDAC, HMT and HDMT gene probes that are either up- or down-regulated, as determined for differentially expressed genes by applying filters described above, are highlighted by yellow and blue colors, respectively.

Dataset S2 Summary (provided as an Excel file):

Log_2 fold change values of *Spo11*$^{-/-}$ versus wild-type B6/DBA expression of differentially expressed genes encoding HAT, HDAC, HMT and HDMT enzymes in spermatogonia, pre-leptotene and leptotene-zygotene meiotic cells. Criteria for defining differentially expressed genes in wild-type meiotic cells are provided in Dataset S1 and in the Materials and Methods. Histone modifying gene probes that are either up- or down-regulated in *Spo11*$^{-/-}$ meiotic cells, based on their fold change values (log_2 ratio ≥0.58 and ≤-0.58), are highlighted by yellow and blue colors, respectively. Corresponding log_2 fold change value of spermatogonia/average pachytene expression defined for each gene probe in wild-type meiotic cells in Dataset S1 is also provided. Log_2 fold change expression values for histone modifying genes in *Spo11*$^{-/-}$ versus wild-type B6/DBA meiotic cells are also plotted in Figs. S6B and D, and S7B and D.

Dataset S3 Summary (provided as an Excel file):

A list of 9R motif sites specific for the PRDM9 9R (C57Bl/6J) allele were identified within the *HS22* hotspot core sequence (9Rc1-9Rc7) and are shown in Fig. S12A. The Dataset S3 Excel Table containing FIMO 9R motif search results has columns with: (1) pattern name; (2) sequence name, genomic coordinate for chromosome 19 (chr19); (3) start; (4) stop; (5) DNA strand; (6) score; (7) p-value; (8) q-value; (9) matched sequence; and (10) 9R motif ID. Applied *p*-value output and score value thresholds were <0.01 and >3.4, respectively. Motifs repeated in the other genomic regions were excluded from the search.

SUPPLEMENTAL TABLES

Supplemental Table S1. qRT-PCR primer pairs for selected significantly changed probe sets of genes encoding HATs and HDACs shown in Fig. 1C.

Forward	Sequence	Reverse	Sequence
Clock/F	ATGAGCACCAAGACCATTCC	*Clock*/R	GCTTCAGTGCTCCCAACTTC
Ncoa1/F	TGGGTACCAGTCACCAGACA	*Ncoa1*/R	GAATGTTTGCGTTTCCACCT
Ncoa3/F	TCAGCGACATCGACAACTTC	*Ncoa3*/R	TCACCACAAACAGGAAACCA
Csrp2bp/// loc1000048645/F	GCCACACCTAGCTTGCTTTC	*Csrp2bp*/// loc1000048645/R	TTCGCTATCTCCATCCATCC
Taf5/F	ATATTTGCTGGCCATCTTGC	*Taf5*/R	TAGCCAGGAATCTCCCATTG
Kat5/F	CAGATCACACTCCGCTTCAA	*Kat5*/R	CTGACCCATTCTGAGGGAAA
Sirt6/F	TCATTGTCTCCACCACAGGA	*Sirt6*/R	AGCATTCTCGAAGGTGGTGT
Crebbp/F	TGGAGTGAACCCCCAGTTAG	*Crebbp*/R	TTGCTTGCTCTCGTCTCTGA
Ep300/F	GCCAAGTATGCCAACCCTAA	*Ep300*/R	TGTTCATTTGCTGAGCTTGG
Sirt1/F	ACACCCTCCCCAAACTGAAT	*Sirt1*/R	GCGTCATATCATCCAGCTCA
Sirt3/F	TCTCACTGCTTCCTCCACCT	*Sirt3*/R	GTTGGTAGTCATGCGTGGTG

Supplemental Table S2. The 48 primer pairs used to tile the *HS59.5* hotspot*

Loc.	Forward	Sequence	Reverse	Sequence
-1705	HS59.5.01/F	CTGGATTGCAAGTGGAGTGAT	HS59.5.01/R	TGGGGGTAGGGAGATAGTTCA
-1598	HS59.5.02/F	CCCTACCCCCATATAAAGCAC	HS59.5.02/R	TTGAACTCAAGCAGCCAGACT
-1583	HS59.5.03/F	ACATGGGCTGGCAAGATGT	HS59.5.03/R	GTGAGTCCCAGGGATTGAACT
-1491	HS59.5.04/F	CCTGGGACTCACATGGTAAAG	HS59.5.04/R	CTTGGCTCCTGATGGTCTTTT
-1386	HS59.5.05/F	GGAGCCAAGACCCAGAGTTTA	HS59.5.05/R	CTCTCTTCCGTCTTTCCAACC
-1123	HS59.5.07/F	CAACAGTAGCAGGATGGGAGA	HS59.5.07/R	GAGACCCATTCTCAACAATAGC
-1001	HS59.5.08/F	CTCACCATGCAAGTCAAGGAT	HS59.5.08/R	TAGAGGTGAACGCCTGTAAGC
-906	HS59.5.09/F	CCAGCTTGTCTGATGCTAAGAA	HS59.5.09/R	CAATATACAAGGGGCTGGAGA
-733	HS59.5.11/F	GGTCTCCTGATGCTCAGGTTC	HS59.5.11/R	GCCTCCTTAAGTGGAGTGGAT
-669	HS59.5.12/F	GGGGCCACAGTATAATCCACT	HS59.5.12/R	CACCTGAGGACCAACAGTGAG
-545	HS59.5.13/F	CGCCATTCACTTATGTTCCA	HS59.5.13/R	CTCGGAGGGAAATACCAAAGA
-456	HS59.5.14/F	CTCCGAGAGAAATGCAGTCAC	HS59.5.14/R	ACCTTCAACCATGTGACCAAG
-443	HS59.5.58/F	AGAAATGCAGTCACCCTTGC	HS59.5.58/R	GCAAAAATCATCCCTCTCCA
-376	HS59.5.59/F	TGGAGAGGGATGATTTTTGC	HS59.5.59/R	CCAGAAGAAATGCAGTTGTGG
-240	HS59.5.61/F	TGACCAAAAAACCACTGTGGAG	HS59.5.61/R	AGACCCACAAACAGCACTGAG
-184	HS59.5.62/F	TCCAGCTCTGAATCCTCACTC	HS59.5.62/R	TTAGACCTGTGCCTTTTGTGG
-95	HS59.5.63/F	AAAGGCACAGGTCTAAAGATGG	HS59.5.63/R	GGTGGGAACCAAAGAAACCT
-69	HS59.5.64/F	CAGAAGGTACTGTCCTCCTAAGAT	HS59.5.64/R	GTCCTTAGTAGATTGTGGGGACAT
59	HS59.5.65/F	GGCCAGAGAGACTTGGTGTC	HS59.5.65/R	CTCATGTGGGAACAGAAATGC
61	HS59.5.66/F	GATTGGCCAGAGAGACTTGGT	HS59.5.66/R	AAGGGAGACTCATGTGGGAAC
130	HS59.5.67/F	GCTGACCTGAGAGCATTTCTG	HS59.5.67/R	GTCTCCTCACCTTGCCAGAC
227	HS59.5.22/F	CGGGTATGTGTGTCAGAGGTC	HS59.5.22/R	CATTCACCCTCCCTTGAAGAT
290	HS59.5.23/F	CTACGAGGCAAATTTCTGAGC	HS59.5.23/R	ACCCCATAGAAGGATGCAAAC
307	HS59.5.24/F	ATCTTCAAGGGAGGGTGAATG	HS59.5.24/R	CTTCAGTCCTGGACCCCATAG
404	HS59.5.25/F	CTGGCTGAGTGTCAGTGTTCA	HS59.5.25/R	ACCAGAGTGCAGTCCATCATC
485	HS59.5.26/F	ATGATGGACTGCACTCTGGTC	HS59.5.26/R	TGCTCTGGATCTTGCTACACA
509	HS59.5.27/F	CCCTTTGAGGATCGTTTGC	HS59.5.27/R	CAGTCTGCTCTGGATCTTGCT
608	HS59.5.29/F	GGAGCACATCCACACTTCTGT	HS59.5.29/R	CACCATGTCACCATCCATACA
867	HS59.5.30/F	CTTGCCCAAGGTTGAAGAGAC	HS59.5.30/R	CTCATACCAAGTCAGGCGTTC
955	HS59.5.32/F	AGTTAAGAGCCAGGGGCAAC	HS59.5.32/R	CAGAGGTGACTGAGCTGGAAG
1048	HS59.5.33/F	ACCTCTGGAAAAGGCTTGATG	HS59.5.33/R	GAACCCTTGTTCTCCCAGTTC
1075	HS59.5.34/F	TCACAAAGATCCTTGAGGCTAC	HS59.5.34/R	CTGGATGGGAACCCTTGTT
1140	HS59.5.35/F	CTCAGAACTGGGAGAACAAGG	HS59.5.35/R	CCTCCTGGCTTGAAAATCTTG
1205	HS59.5.36/F	GGGTGGAGAGAGGCAAGATT	HS59.5.36/R	ATAGATGAGACGGTGCCAAGA
1206	HS59.5.37/F	GGTGGAGAGAGGCAAGATTTTC	HS59.5.37/R	TATAGATGAGACGGTGCCAAGA
1288	HS59.5.38/F	GGCACCGTCTCATCTATATGTC	HS59.5.38/R	CAGGCATGTGACCAGTTTAGTT
1385	HS59.5.39/F	CTGCACCTCCTTGCTTAACTG	HS59.5.39/R	CCATGTACTTCCCGATTGTT
1433	HS59.5.40/F	GATGTGTTCTCGTTGTCAGCA	HS59.5.40/R	GTAGGACCAGAAAGGGGACCT
1512	HS59.5.41/F	TCCCCTTTCTGGTCCTACAAC	HS59.5.41/R	GCAGACCTTGATGGAAACTTG
1552	HS59.5.42/F	CTTAGCGCAAACCTCTCCAG	HS59.5.42/R	AAACGCCATTTGTCTGTGTG
1633	HS59.5.44/F	CAAATGGCGTTTGTTTCAGC	HS59.5.44/R	ACCCCAACATGAGGAACTGTA
1943	HS59.5.46/F	ATATCTTCCCCCACGATCCTT	HS59.5.46/R	TTAGTAGGAGGTTCGCCTTGA
2122	HS59.5.49/F	GTCAGCCAGCTGCCCTACT	HS59.5.49/R	ATGTCACATGAGGCACCATTC
2169	HS59.5.50/F	TCTCCTATTACATCCCCAGTGC	HS59.5.50/R	GATCTTTCTCCTACGGCCAAT
2314	HS59.5.53/F	CAAGGGCATTTTTGACTTCC	HS59.5.53/R	CCTCCCAAACCCTGACTTTAG

2406	HS59.5.54/F	GGGAGGCAAAGGTCAAAGT	HS59.5.54/R	AACTCGGGCGCTGTTACTTAT
2626	HS59.5.56/F	TCTGGTGGTTTTTCCTGTGTC	HS59.5.56/R	GAACAGCCAGTAGCTGAATGC
2658	HS59.5.57/F	GAGAAAGCTACCCCTGCATTC	HS59.5.57/R	AAGCCCTTGCTACACAAACCT

*The sequence of the forward and reverse pair are provided for each surveyed amplicon, along with their distance (Loc.) from the center of the core of the hotspot in base pairs.

Supplemental Table S3. Summary of sperm CO data at the *HS59.5* hotspot

Hotspot	Orientation	Number of amplifiable molecules	Number of COs detected	Rate ($x10^{-4}$) [95% CI]
HS59.5	B->D	224686	44	1.96 [1.14-2.78]
	D->B	224686	56	2.49 [1.57-3.42]
	Both	449372	100	2.23

Supplemental Table S4. Summary of effects of HAT and HDAC inhibitors on CO rates at two mouse meiotic recombination hotspots

Inhibitor compound used *in vivo* treatment	Hotspot	Orientation	Number of amplifiable molecules	Number of COs detected	Rate ($x10^{-4}$) [95% CI]*
S2	*HS59.5*	D->B	1630	9	55.20 [41.87-68.53]
S2	*HS22*	D->B	4176	13	31.13 [22.51-39.75]
Liposomal 2c	*HS59.5*	D->B	58823	1	0.17 [0.08-0.27]
Liposomal 2c	*HS22*	D->B	166667	2	0.12 [0.04-0.20]

*Results are means and s.e.m. for biological replicates (n = 3).

SUPPLEMENTAL FIGURE LEGENDS

Supplemental FIG S1 Profiles of active and repressive histone H3 and H4 acetylated and methylated marks at *HS22* at the pachytene/diplotene stage of meiosis I. (A) Representative normalized native ChIP profiles of the active acetylated histone H4 (H4K12Ac) and methylated histone H3 (H3K4Me3) marks are shown at the pachytene-diplotene meiotic stage for the *HS22* hotspot. Histone modification profiles for these marks at earlier meiotic stages at the *HS22* hotspot are shown in Fig. 2. (B) Representative normalized native ChIP profiles of repressive methylated histone H3 (H3K9Me3, H3K27Me3) marks are shown at the pachytene-diplotene meiotic stage for the *HS22* hotspot. Histone modification profiles for these marks at earlier meiotic stages at the *HS22* hotspot are shown in Fig. 4A. (A and B) Normalized histone modification profiles were obtained as in Fig. 2 legend. Each of the ChIP profiles shown is the average of three independent, normalized ChIP experiments. Statistical significance of the histone mark enrichments (if any) within the *HS22* hotspot core and *p*-values were defined using Mann-Whitney test as in the legend for Fig. 2; *, $p<0.05$. *HS22* hotspot cores are indicated with red shading.

Supplemental FIG S2 Superposition of H3K4Me3 mark ChIP profiles with nucleosome occupancy maps at four meiotic hotspots. (A) An overlay of non-normalized native ChIP profiles of the active H3K4Me3 histone mark in spermatogonia, pre-leptotene and leptotene-zygotene meiotic cells, with nucleosome occupancy profiles obtained by either real-time PCR (1, 2) (*black* and *white panels*) or by whole genome sequencing (WGS)

(*bottom panels*) at *HS22, HS59.4, HS59.5* and *HS61.1* hotspots is shown. Normalized native ChIP H3K4Me3 profiles at these hotspots are shown in Fig. 2. In ChIP panels, the *y*-axis scale indicates the absolute fold enrichment between bound and input ChIP DNA fractions, calculated using the $2^{-\Delta Ct}$ formula, for validated primer pairs that overlap these hotspots (see Materials and Methods and Fig. 2B). Nucleosome occupancy profiles were generated by micrococcal nuclease (MNase) digestion of native chromatin, followed by either real-time PCR analysis (1, 2) (see also Fig. 2B) or by WGS of mono-nucleosomal DNA isolated from the total meiotic fraction (see Fig. S3B and C). Real-time PCR nucleosome maps are averaged by all meiotic stages, with the *y*-axis scale normalized to the highest peak fold enrichment between the mono-nucleosome MNase-digested DNA fraction and undigested genomic DNA, calculated using the $2^{-\Delta Ct}$ formula. The *x*-axis represents the location across the analyzed *HS* locus. *ChIP enrichment value for this peak is 13.2. Hotspot cores, red shading. *Bottom panels*, WGS hotspot nucleosome maps validated the real-time PCR and nucleosome occupancy profiles throughout meiosis. In WGS panels, the *y*-axis scale indicates sequence reads, the *x*-axis represents genomic position of a hotspot on chromosome 19 (chr 19). Coding transcripts and gene names are indicated. Notably, nearly all of the nucleosome peaks obtained in real-time PCR profiles co-localize with whole genome sequencing tags, excluding a few gap regions either containing repeats where primer pairs could not be designed or where there was poor efficiency of selected primers. (B) FACS profile showing total meiotic cell fraction purification that was used for native chromatin isolation (Sp – Spermatogonia, pL – pre-Leptotene, L/Z – Leptotene-Zygotene, P/D – Pachytene-Diplotene). (C) Mono-nucleosomal DNA band that was used to generate the Illumina library and WGS data (details are provided in Materials and Methods).

Supplemental FIG S3 Profiles of active histone H3 and H4 acetylated and methylated marks at *HS22* hotspot locus and surrounding *HS22* hotspot flanking regions. Normalized native ChIP profiles of H4K12Ac (*top*) and H3K4Me3 (*middle*) marks are shown at 1 kb intervals in regions flanking *HS22* hotspot, at -25, -10, +10, and +25 kb from the *HS22* hotspot core center, in spermatogonia, pre-leptotene and leptote-zygotene meiotic stage cells. Corresponding histone H4K12Ac and H3K4Me3 mark profiles at the *HS22* hotspot region are shown for comparison in the center. *Bottom panels*, genome-wide profiles of the active histone H3K4Me3 mark and meiotic DSBs in total germ cells isolated from C57BL/6J wild-type mouse testis at *HS22* hotspot region and at corresponding 1 kb regions flanking -25, -10, +10, and +25 kb *HS22* hotspot core regions are shown for comparison. WGS data were adapted from published H3K4Me3 ChIP-Seq and DMC1 Single-Stranded DNA Sequencing (SSDS) datasets (GEO accession numbers are GSM869792 and GSM869781, respectively)(3). Normalized native ChIP profiles (*top* and *middle panels*) were obtained from real-time PCR data analysis using validated primer pairs across *HS22* hotspot and the 1 kb flanking regions that are -25, -10, +10, and +25 kb from the *HS22* hotspot core (1) as described in Materials and Methods. The *y*-axis scale indicates the normalized ratios of bound native ChIP fractions of a given histone mark versus no antibody control, using $2^{-\Delta\Delta Ct}$ formula. The *x*-axis represents the location across the *HS22* locus. In genome-wide profiles (*bottom panels)*, the *y*-axis scale indicates sequence reads, the *x*-axis represents genomic position of a hotspot on chromosome 19 (chr 19). The coding *Trpm3* transcript found within the *HS22* hotspot locus and *HS22* flanking regions is also indicated. WGS images were generated using Integrative Genomic Viewer (IGV 2.3) software. The *HS22* hotspot core region is depicted with the red bar.

Supplemental FIG S4 Non-normalized native ChIP profiles of the active H4K5Ac and H4K8Ac histone marks (*top panels*), the active H4K12Ac and H3K4Me3 histone marks (*middle panels*), and the repressive H3K27Me3 and H3K9Me3 histone marks (*bottom panels*) in spermatogonia, pre-leptotene and leptotene-zygotene meiotic cells at the *HS22* hotspot in inactive (CAST/DBA) versus active (B6/DBA) mouse strains. Native ChIP profiles were obtained by calculating the absolute fold enrichment between bound and input ChIP DNA fractions, using the $2^{-\Delta Ct}$ formula (see Materials and Methods and Fig. 2B). Each of the ChIP profiles shown is the average of three independent ChIP experiments. Inactive and active *HS22* hotspot cores in CAST/DBA and B6/DBA mice are indicated with blue and red shading, respectively. Corresponding normalized histone mark profiles in CAST/DBA versus B6/DBA strain backgrounds are shown in Fig. 5.

Supplemental FIG S5 Non-normalized nChIP profiles of the active and repressive methylated H3K4Me3 and H3K27Me3 histone marks (*top panels*), and of the active acetylated H4K12Ac and H4K16Ac histone marks (*bottom panels*) in spermatogonia, pre-leptotene and leptotene-zygotene meiotic cells, is shown at the *HS22* hotspot in *Spo11*$^{-/-}$ and wild-type B6/DBA mice. Native ChIP profiles were obtained by calculating the absolute fold enrichment between bound and input ChIP DNA fractions, using the $2^{-\Delta Ct}$ formula (see Materials and Methods and Fig. 2B). *ChIP enrichment value for this peak is 13.2. The hotspot core present at *HS22* in B6/DBA mice is indicated with red shading in each of the shown ChIP profiles. Each of the ChIP profiles shown is the average of at least two independent ChIP experiments. Corresponding normalized histone mark profiles in *Spo11*$^{-/-}$ versus B6/DBA mice are shown in Fig. 6.

Supplemental FIG S6 Expression of genes encoding histone methylases and demethylases in early meiotic cells from *Spo11*$^{-/-}$ mice. (A) Profiling of genes encoding histone methylases (defined as differentially expressed in wild-type mice, Fig. 1) in *Spo11*$^{-/-}$ spermatogonia, pre-leptotene and leptotene-zygotene-like meiotic stage cells. (B) Scatter plot representation, in $\log_2$ scale, of *Spo11*$^{-/-}$ versus wild-type B6/DBA expression ratios for the HMT gene probes shown in the heatmap of (A), in spermatogonia (red squares), pre-leptotene (green triangles) and leptotene-zygotene (purple circles) meiotic cells. (C) Profiling of genes encoding histone demethylases (again defined as differentially expressed in wild-type mice, Fig. 1) in *Spo11*$^{-/-}$ spermatogonia, pre-leptotene and leptotene-zygotene-like meiotic stage cells. (D) Scatter plot representation, in $\log_2$ scale, of *Spo11*$^{-/-}$ versus wild-type B6/DBA expression ratios for HDMT gene probes shown in the heatmap of (C), in spermatogonia (red squares), pre-leptotene (green triangles) and leptotene-zygotene (purple circles) meiotic cells. (A and C) An absolute fold change filter of 1.5-fold for spermatogonia/average pachytene expression ratio from wild-type mice (see Fig. 1) was applied to obtain the differentially expressed gene list followed by hierarchical clustering. Only significantly changed probe sets with p-value (corrected) <0.05 are shown. The expression of HMTs and HDMTs in three *Spo11*$^{-/-}$ (*left*) and wild-type B6/DBA (*right*) meiosis I stage cells is shown in each of the heatmaps in (A) and (C). Respective $\log_2$ values of wild-type spermatogonia/average pachytene (Log2(Sp/AvP)) expression ratios for each of the HMT and HDMT gene probes in (A) and (C) are plotted in (B) and (D) and are depicted with blue circles. Microarray data were normalized across the median for all wild-type and *Spo11*$^{-/-}$ samples; microarray analysis is described in Materials and Methods. Details of statistical analysis are provided in Dataset S1. Actual values of gene expression

ratios plotted in (B) and (D) are also shown in Dataset S2, where up- and down-regulated HMT and HDMT gene probes in *Spo11*$^{-/-}$ are highlighted in different colors.

Supplemental FIG S7 Expression of genes encoding histone acetylases and deacetylases in early meiotic cells from *Spo11*$^{-/-}$ mice. (A) Profiling of genes encoding HATs (defined as differentially expressed in wild-type mice, Fig. 1) in *Spo11*$^{-/-}$ spermatogonia, pre-leptotene and leptotene-zygotene-like meiotic stage cells. (B) Scatter plot representation, in $\log_2$ scale, of *Spo11*$^{-/-}$ versus wild-type expression ratios for the HAT gene probes shown in the heatmap in (A), in spermatogonia (red squares), pre-leptotene (green triangles) and leptotene-zygotene (purple circles) meiotic cells. (C) Profiling of genes encoding HDACs (again defined as differentially expressed in wild-type mice, Fig. 1) in *Spo11*$^{-/-}$ spermatogonia, pre-leptotene and leptotene-zygotene-like meiotic stage cells. (D) Scatter plot representation, in $\log_2$ scale, of *Spo11*$^{-/-}$ versus wild-type B6/DBA expression ratios for the HDAC gene probes shown in the heatmap of (C), in spermatogonia (red squares), pre-leptotene (green triangles) and leptotene-zygotene (purple circles) meiotic cells. (A and C) An absolute fold change filter of 1.5-fold for spermatogonia/average pachytene expression ratio from wild-type mice (see Fig. 1) was applied to obtain the differentially expressed gene list followed by hierarchical clustering. Only significantly changed probe sets with p-value (corrected) <0.05 are shown. Expression of HATs and HDACs in three *Spo11*$^{-/-}$ (*left*) and wild-type B6/DBA (*right*) meiosis I stage cells is shown in the heatmaps in (A) and (C). Respective $\log_2$ values of wild-type spermatogonia/average pachytene expression ratios (Log2(Ap/SvP)) for the HAT and HDAC gene probes in (A) and (C) are plotted in (B) and (D) and are depicted with blue circles. Microarray data were normalized across the median

for all wild-type and *Spo11*$^{-/-}$ samples; microarray analysis is described in Materials and Methods. Details of statistical analysis are provided in Dataset S1. Actual values of gene expression ratios plotted in (B) and (D) are also shown in Dataset S2, where up- and down-regulated HAT and HDAC gene probes in *Spo11*$^{-/-}$ are highlighted in different colors.

Supplemental FIG S8 Effects of HDAC and HAT inhibitors on meiosis and on global levels of acetylated histones. (A) Structures of the HDAC inhibitor s2 (*left*) and the HAT inhibitor 2c (*right*). (B) *Top panels*, FACS profiles were performed on meiotic cells isolated from the testes of drug- and vehicle-treated mice to assess potential effects on meiosis. Mice were treated with the HDAC inhibitor s2 (1 mg/kg) or vehicle (*left panels)*, or with liposomal HAT inhibitor 2c (50 mg/kg) or vehicle (*right panels)*, meiotic cells were isolated and analyzed by FACS. *Bottom tables*, percentages of each population in vehicle- and inhibitor-treated mice. Sp – Spermatogonia, pL – pre-Leptotene, L/Z – Leptotene-Zygotene, P/D – Pachytene-Diplotene. (C) Effects of the HDAC inhibitor s2 on the total levels of acetylated histone H3 in meiotic cells. Male mice were treated with the s2 compound, meiotic cells were isolated and levels of Ac-H3 and total H3 were determined by immunoblot analyses. (D) Effects of the HAT inhibitor 2c on the total levels of acetylated histone H3 and H4. Mice were treated with the 2c compound, meiotic cells were isolated and levels of Ac-H3, Ac-H4, total H3 and total H4 were determined by immunoblot analyses. (C and D) Equal loading was confirmed by immunoblotting with antibody to β-actin.

Supplemental FIG S9 Non-normalized nChIP profiles of active acetylated H4K16Ac (*top*), H3K9/14Ac (*middle*) and methylated H3K4Me3 (*bottom*) histone marks at the *HS22*

hotspot in spermatogonia, pre-leptotene and leptotene-zygotene stage meiotic cells from 10-week old B6/DBA mice treated *i.p.* with the HDAC inhibitor s2 (*left panels*) and vehicle (*right panels*). Native ChIP profiles were obtained by calculating the absolute fold enrichment between bound and input ChIP DNA fractions, using the $2^{-\Delta Ct}$ formula (see Materials and Methods and Fig. 2B). *ChIP enrichment value for this peak is 13.2. Red shading indicates the s2-activated and vehicle-treated *HS22* hotspot core. Corresponding normalized histone mark profiles of *i.p.* treated s2 compound versus vehicle B6/DBA mice are shown in Fig. 7A.

Supplemental FIG S10 Non-normalized nChIP profiles of active acetylated H4K12Ac (*top*), active methylated H3K4Me3 (*middle*) and inactive methylated H3K27Me3 (*bottom*) histone marks at the *HS22* hotspot in spermatogonia, pre-leptotene and leptotene-zygotene stage cells from 10-week old B6/DBA mice treated *i.p.* with the HAT inhibitor 2c (*left panels*) and vehicle (*right panels*). Native ChIP profiles were obtained by calculating the absolute fold enrichment between bound and input ChIP DNA fractions, using the $2^{-\Delta Ct}$ formula (see Materials and Methods and Fig. 2B). Blue shading indicates the 2c-inactivated *HS22* hotspot core. Red shading indicates original vehicle treated *HS22* hotspot core. Corresponding normalized histone mark profiles of *i.p.* treated 2c compound versus vehicle B6/DBA mice are shown in Fig. 7C.

Supplemental FIG S11 Effects of HDAC and HAT inhibitors treatments on histone acetylation marks levels at *HS59.5* and *HS22* hotspots in B6/DBA and CAST/DBA mice backgrounds. (A) Normalized log2 (ΔΔCt) native ChIP analyses of active acetylated

H4K16Ac, H3K9/14Ac and methylated H3K4Me3 histone marks were performed for the *HS59.5* hotspot in spermatogonia, pre-leptotene and leptotene-zygotene stage meiotic cells from 10-week B6/DBA mice treated *i.p.* (1mg/kg) with the HDAC inhibitor s2 versus vehicle. Red shading indicates the s2-activated *HS59.5* hotspot core. (B) Normalized log2 (ΔΔCt) native ChIP analyses of the active H4K12Ac histone mark were performed for the *HS22* hotspot in spermatogonia, pre-leptotene and leptotene-zygotene stage cells from 10-week CAST/DBA mice treated *i.p.* (1mg/kg) with the HDAC inhibitor s2 versus vehicle. Blue shading indicates an inactive *HS22* hotspot core in CAST/DBA mouse background. (C) Normalized log2 (ΔΔCt) native ChIP analyses of the active H4K12Ac and repressive H3K27Me3 histone marks were performed for the *HS59.5* hotspot in spermatogonia, pre-leptotene and leptotene-zygotene stage cells from 10-week old B6/DBA mice treated *i.p.* (50 mg/kg) with the HAT inhibitor 2c versus vehicle. Blue shading indicates the 2c-inactivated *HS59.5* hotspot core. Normalization method and inhibitor treatment details for (A-C) are described in Materials and Methods. Data shown are the average of at least two independent, normalized ChIP experiments. Mann-Whitney test was performed to determine the statistical significance of the difference in normalized bound fraction of a given histone mark within *HS59.5* (A) or *HS22* (B) hotspot core region, or within a specific hotspot core subregion, indicated with a bar, in the s2- and vehicle treated B6/DBA (A) or CAST/DBA (B) mice, respectively, or within *HS59.5* hotspot core in the 2c- and vehicle treated B6/DBA mice (C), as described in Materials and Methods. Corresponding *p*-values are depicted for each of the histone marks in (A-C) at *HS22* hotspot core in three meiotic cell stages; *, $p<0.05$; **, $p<0.01$.

Supplemental FIG S12 Additional data supporting proposed model of meiotic hotspot activation by histone acetylation (Fig. 8). (A) Nucleosome occupancy and the distribution of PRDM9 binding motifs at the *HS22* hotspot. Superposition of *HS22* CO profile (4, 5) (*top*) and genome-wide nucleosome occupancy profile at *HS22* core (*bottom*). B6-to-DBA (red) and DBA-to-B6 (black) CO profiles are shown as a mirror representation. Recombination rate is indicated in the top right corner. The *x*-axis represents location across the *HS22* locus. Putative binding sites for PRDM9 within *HS22* core are indicated with red vertical lines and were obtained from *HS22* sequence scan for the presence of consensus 9R motif sites (3) (*middle*) specific for PRDM9 9R (C57Bl/6J) allele as described in Materials and Methods (see also Dataset 3). Statistically significant 9R motif hits with p value <0.01 (**), <0.001 (***) and <0.0001 (****) are shown by red arrows in genome-wide *HS22* core nucleosome profile and are indicated by the 9Rc1-9Rc7 numeration. Importantly, all identified PRDM9 recognition sites were located next to highly recombined regions. Nucleosomes are indicated by black (located in the vicinity of) and grey (lacking PRDM9 recognition motif) circles and are drawn to scale. *Bottom*, in the WGS data, the *y*-axis scale indicates sequence reads, the *x*-axis represents genomic position of the *HS22* hotspot on chromosome 19 (chr 19). (B) Schematic showing the dynamics ł of active acetylated and methylated histone marks at the *HS22* core throughout early meiosis I. Levels of histone H4 K5, K8, K12, K16 and K91, and of histone H3 K9, acetylated marks levels are shown above the meiotic stages; levels of histone methylated H3K4Me2, K4Me3, K36Me3 and K79Me1 marks changes are drawn below meiotic stages (Sp – Spermatogonia, pL – pre-Leptotene, L/Z – Leptotene-Zygotene, P/D – Pachytene-Diplotene). Full ChIP profiles across *HS22* locus for these histone marks are shown in Figs. 2, 3 and Fig. S1A.

SUPPLEMENTAL REFERENCES

1.**Getun IV, Wu ZK, Khalil AM, Bois PR.** 2010. Nucleosome occupancy landscape and dynamics at mouse recombination hotspots. EMBO Rep **11:**555-560.

2.**Getun IV, Wu ZK, Bois PRJ.** 2012. Organization and roles of nucleosomes at mouse meiotic recombination hotspots. Nucleus **3:**244-250.

3.**Brick K, Smagulova F, Khil P, Camerini-Otero RD, Petukhova GV.** 2012. Genetic recombination is directed away from functional genomic elements in mice. Nature **485:**642-645.

4.**Bois PR.** 2007. A Highly Polymorphic Meiotic Recombination Mouse Hotspot Exhibits Incomplete Repair. Mol Cell Biol **27:**7053-7062.

5.**Wu ZK, Getun IV, Bois PR.** 2010. Anatomy of mouse recombination hot spots. Nucleic Acids Res **38:**2346-2354.

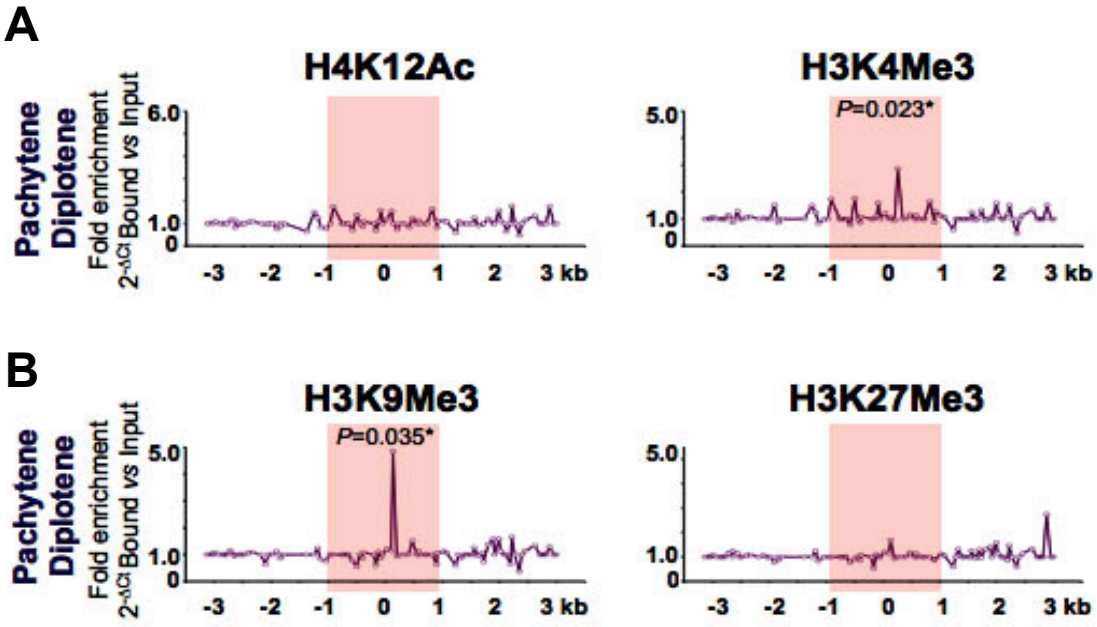
A
H4K12Ac
H3K4Me3
P=0.023*
Pachytene
Diplotene
Fold enrichment
2-ΔCt Bound vs Input
6.0
5.0
1.0
0
-3
-2
-1
0
1
2
3 kb
B
H3K9Me3
P=0.035*
H3K27Me3

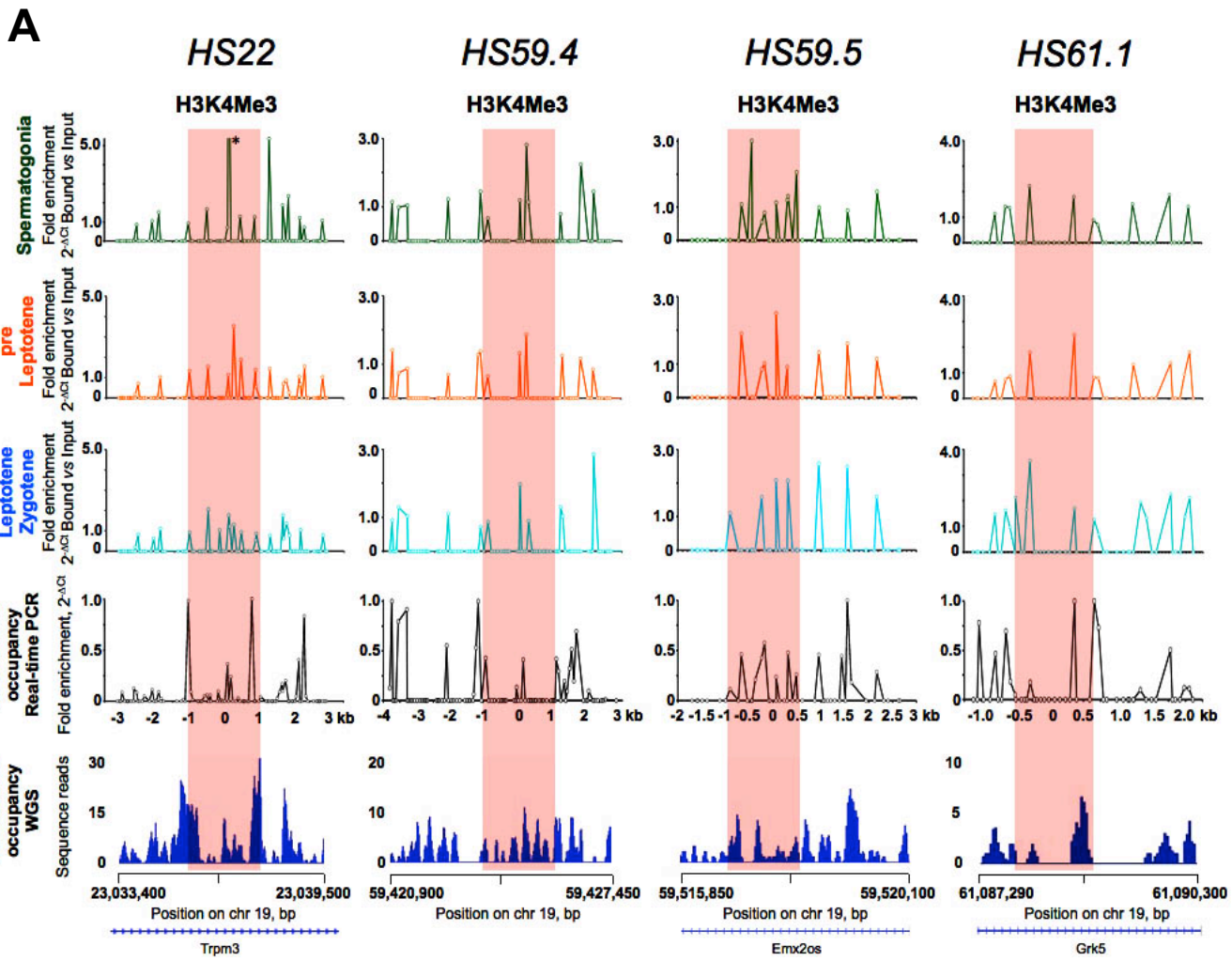
A
HS22
HS59.4
HS59.5
HS61.1
H3K4Me3
Spermatogonia
pre Leptotene
Leptotene Zygotene
Fold enrichment Bound vs Input 2^-ΔCt
Nucleosome occupancy Real-time PCR
Fold enrichment, 2^-ΔCt
Nucleosome occupancy WGS
Sequence reads
23,033,400
23,039,500
59,420,900
59,427,450
59,515,850
59,520,100
61,087,290
61,090,300
Position on chr 19, bp
Trpm3
Emx2os
Grk5

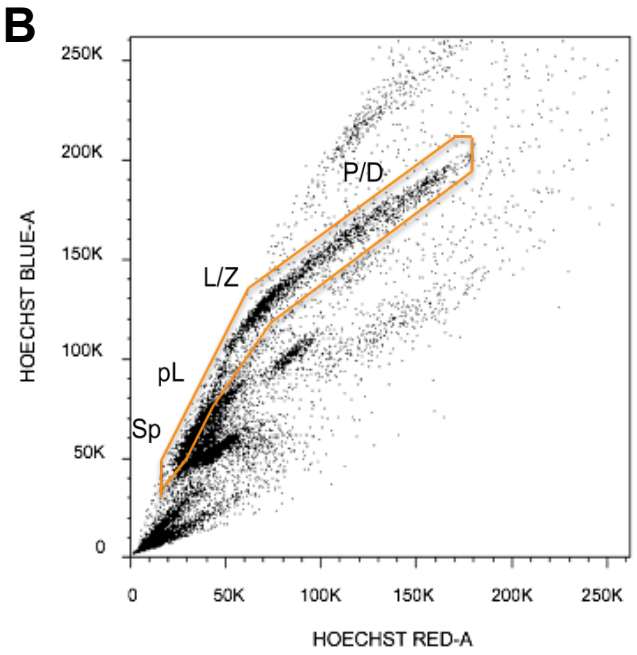
B
HOECHST BLUE-A
HOECHST RED-A
P/D
L/Z
pL
Sp

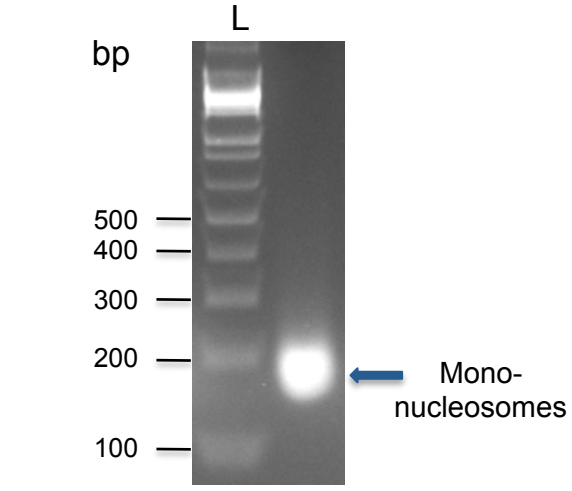
C
L
bp
500
400
300
200
100
Mono-nucleosomes

Getun *et al.* Figure S3

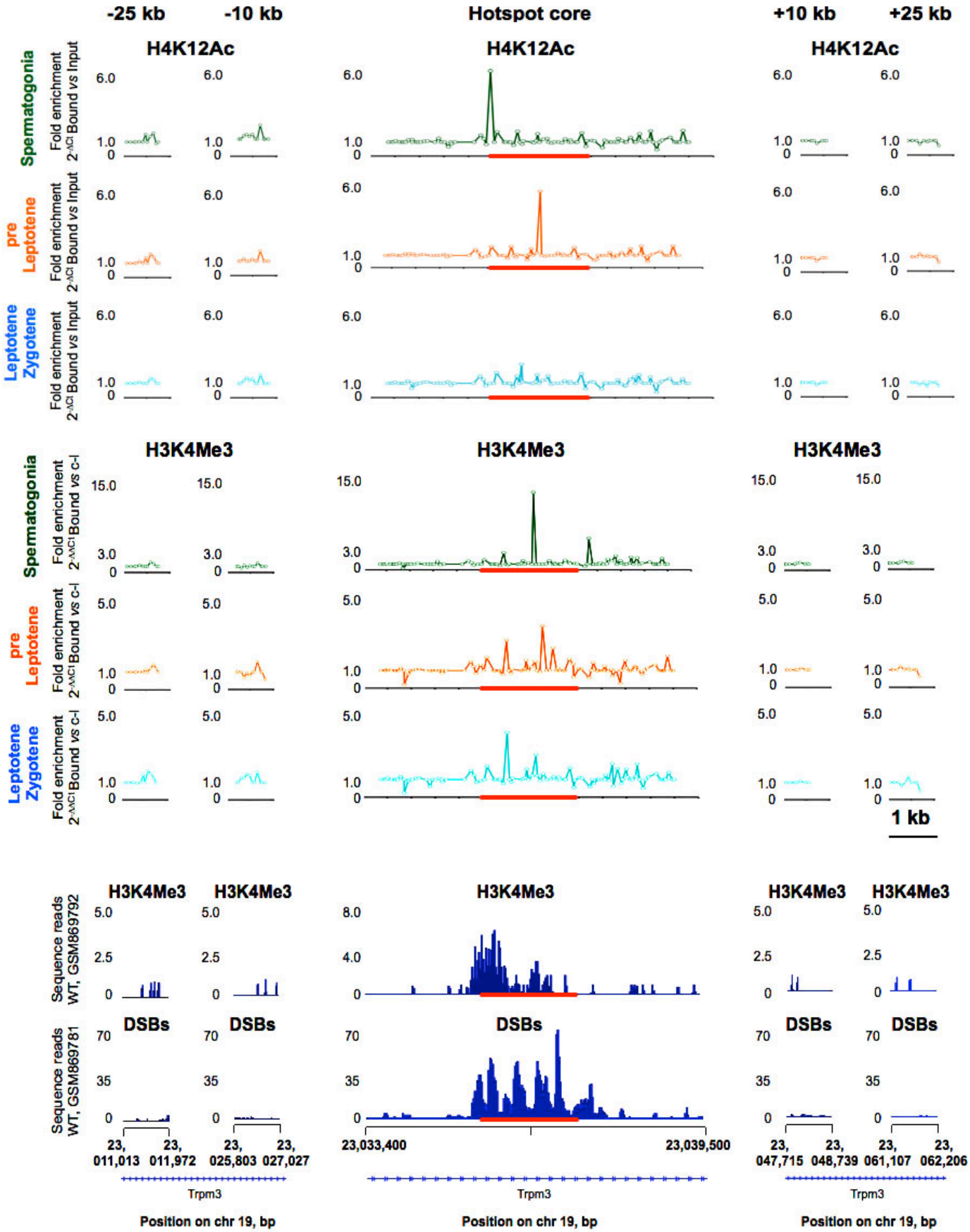

Getun *et al.* Figure S4

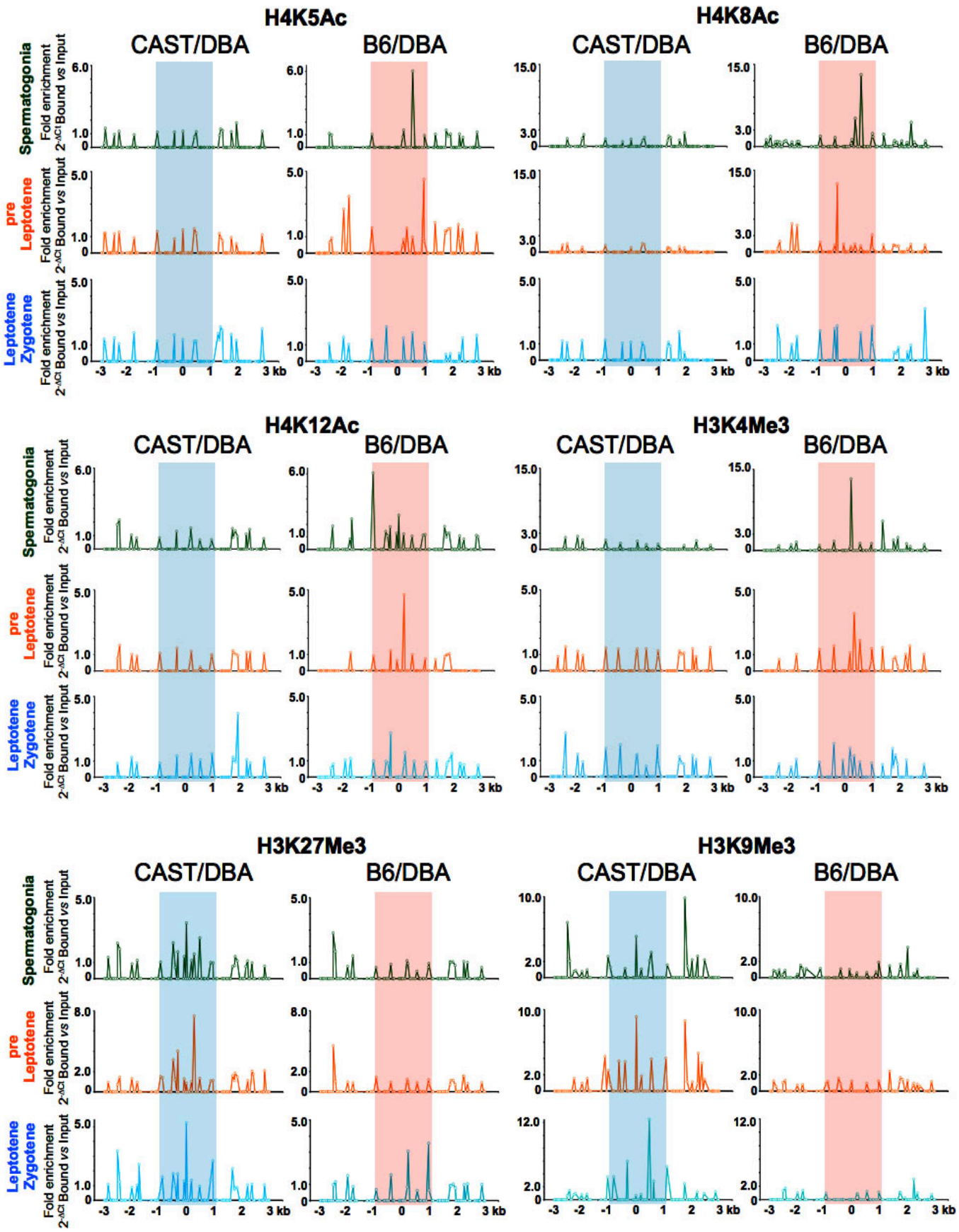

Getun *et al.* Figure S5

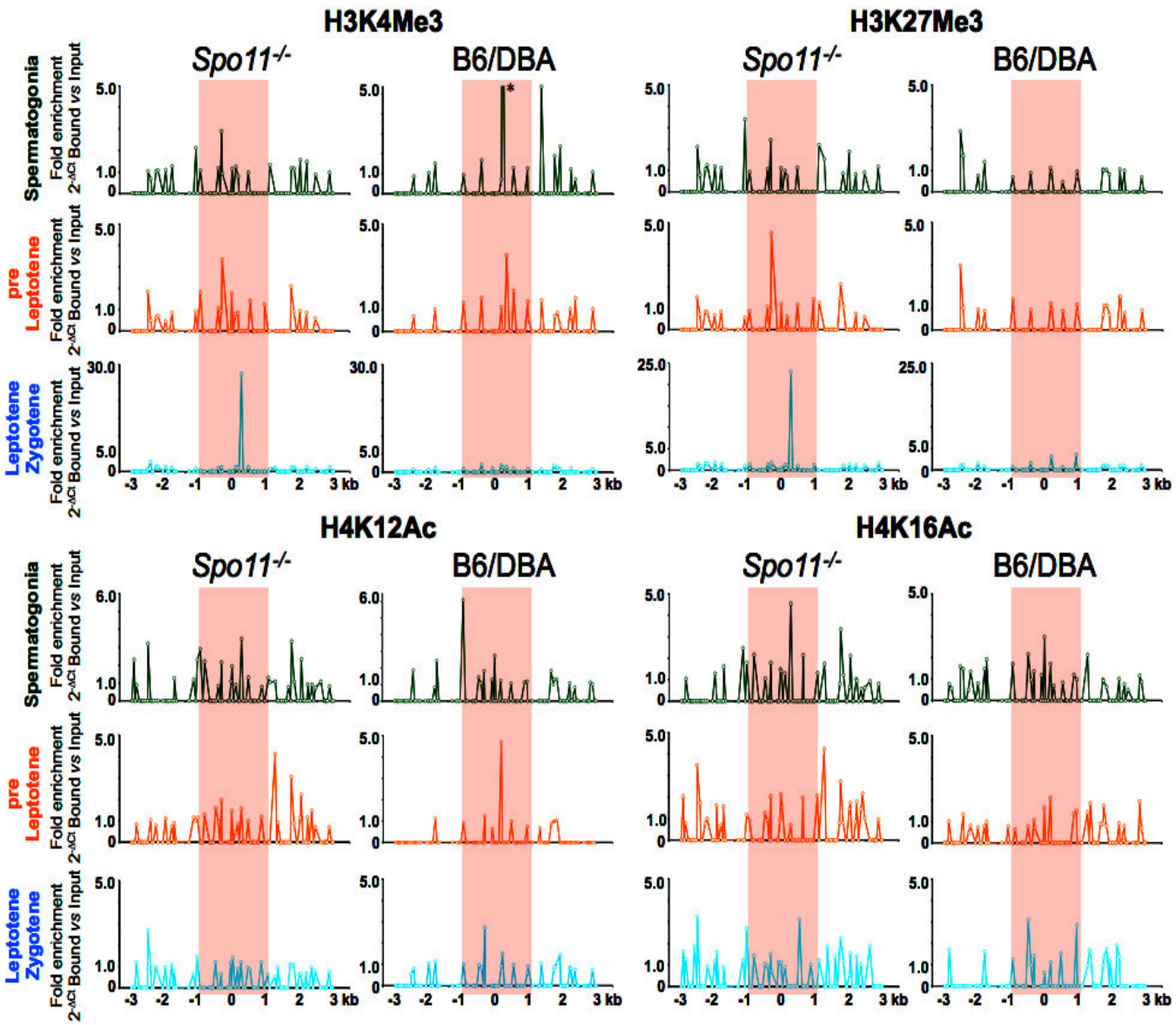

A

Histone methylases

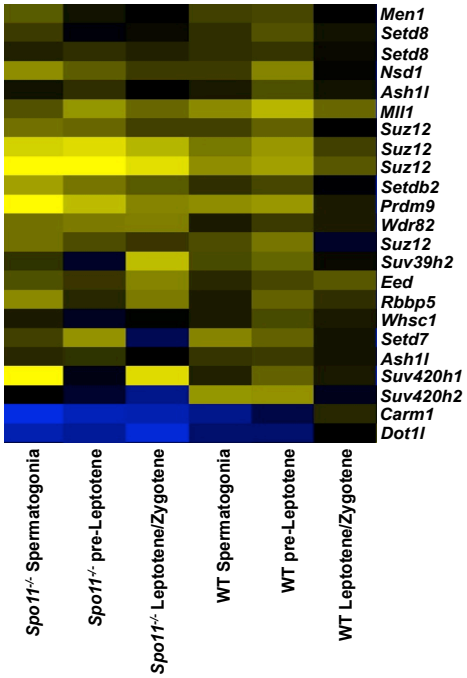

B

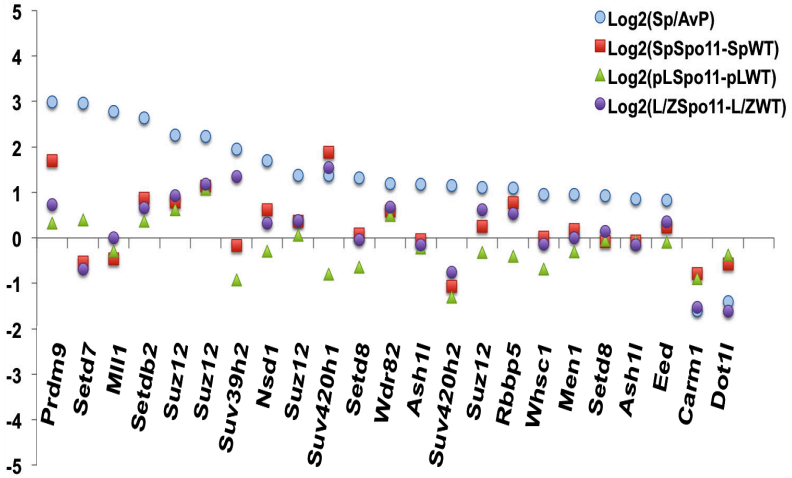

C

Histone demethylases

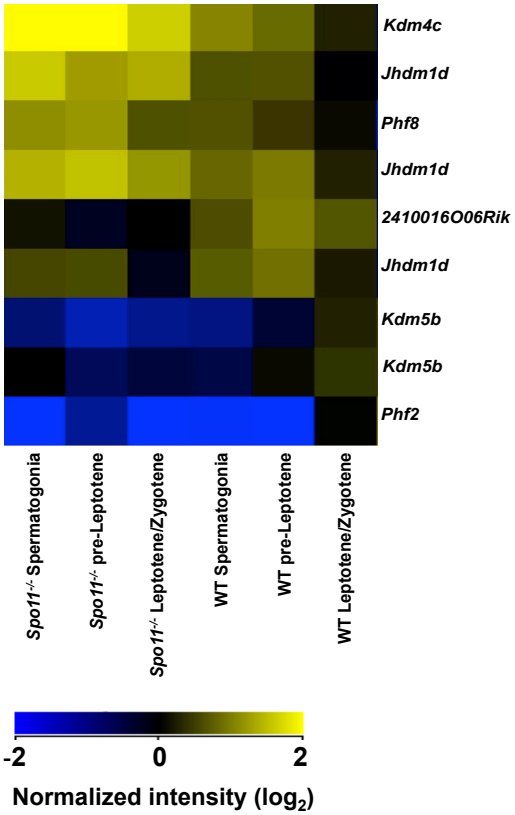

D

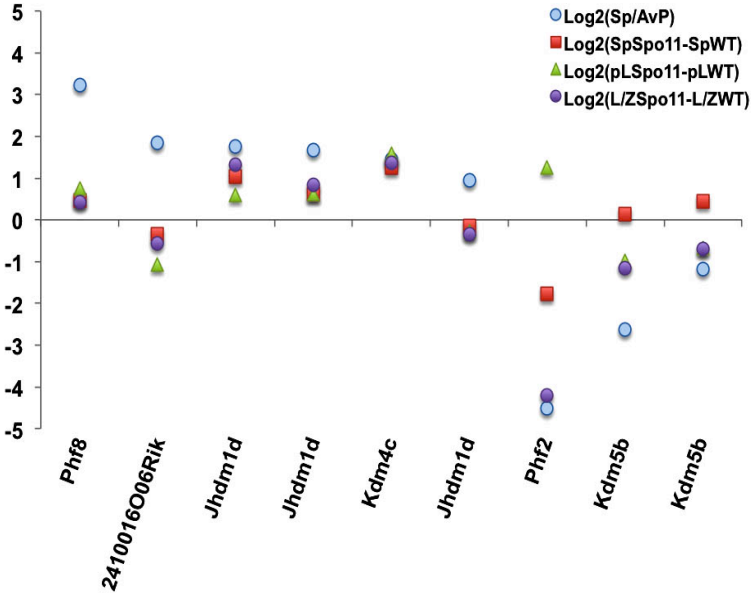

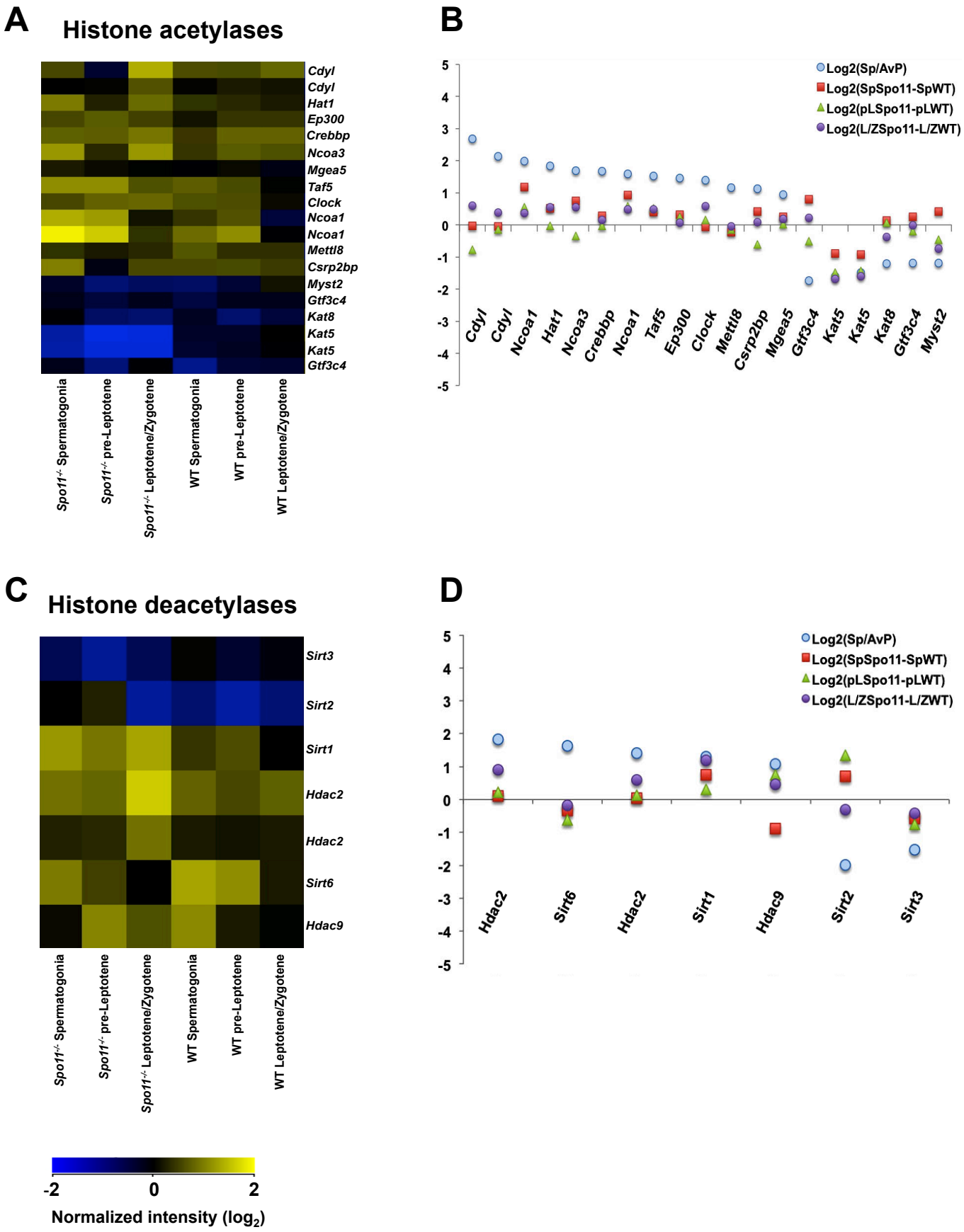
A
Histone acetylases
Cdyl
Cdyl
Hat1
Ep300
Crebbp
Ncoa3
Mgea5
Taf5
Clock
Ncoa1
Ncoa1
Mettl8
Csrp2bp
Myst2
Gtf3c4
Kat8
Kat5
Kat5
Gtf3c4
Spo11-/- Spermatogonia
Spo11-/- pre-Leptotene
Spo11-/- Leptotene/Zygotene
WT Spermatogonia
WT pre-Leptotene
WT Leptotene/Zygotene
B
Log2(Sp/AvP)
Log2(SpSpo11-SpWT)
Log2(pLSpo11-pLWT)
Log2(L/ZSpo11-L/ZWT)
5
4
3
2
1
0
-1
-2
-3
-4
-5
Cdyl
Cdyl
Ncoa1
Hat1
Ncoa3
Crebbp
Ncoa1
Taf5
Ep300
Clock
Mettl8
Csrp2bp
Mgea5
Gtf3c4
Kat5
Kat5
Kat8
Gtf3c4
Myst2
C
Histone deacetylases
Sirt3
Sirt2
Sirt1
Hdac2
Hdac2
Sirt6
Hdac9
Spo11-/- Spermatogonia
Spo11-/- pre-Leptotene
Spo11-/- Leptotene/Zygotene
WT Spermatogonia
WT pre-Leptotene
WT Leptotene/Zygotene
-2
0
2
Normalized intensity (log2)
D
Log2(Sp/AvP)
Log2(SpSpo11-SpWT)
Log2(pLSpo11-pLWT)
Log2(L/ZSpo11-L/ZWT)
5
4
3
2
1
0
-1
-2
-3
-4
-5
Hdac2
Sirt6
Hdac2
Sirt1
Hdac9
Sirt2
Sirt3

Getun *et al.* Figure S8

A

s2 - HDAC inhibitor

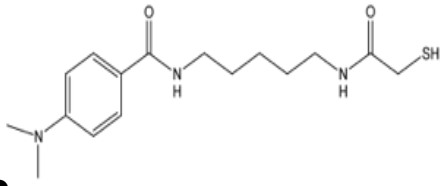

2c - HAT inhibitor

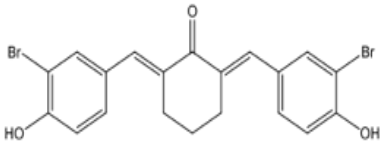

B

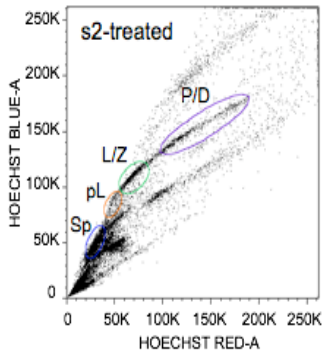

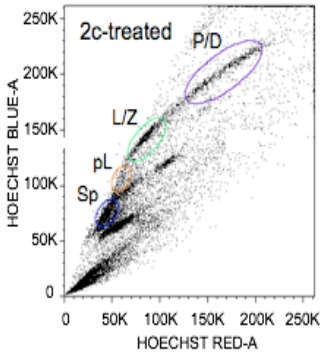

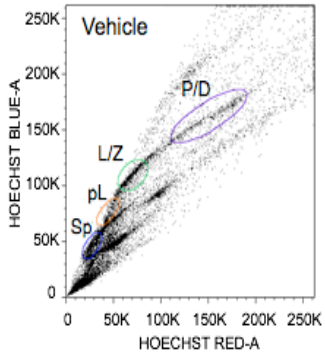

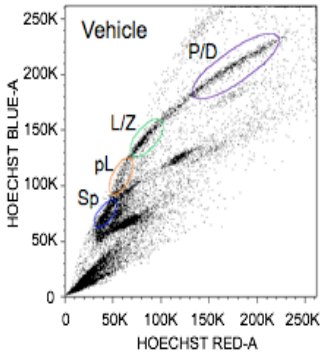

C

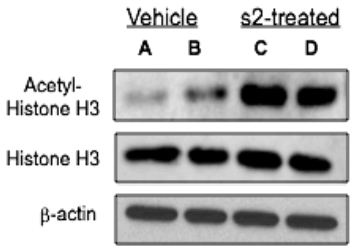

A, B - DMSO/saline vehicle
C, D - treated mice

D

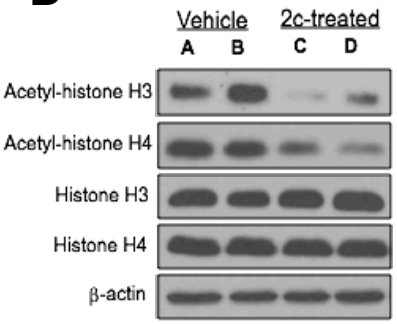

A, B - empty liposome vehicle
C, D - treated mice

	s2-treated Population, %	**Vehicle Population, %**
Sp	24.4	28.3
pL	9.0	12.1
L/Z	40.9	35.0
P/D	25.7	24.6

	2c-treated Population, %	**Vehicle Population, %**
Sp	21.9	22.8
pL	10.0	11.9
L/Z	33.0	27.6
P/D	35.1	37.7

Getun *et al.* Figure S9

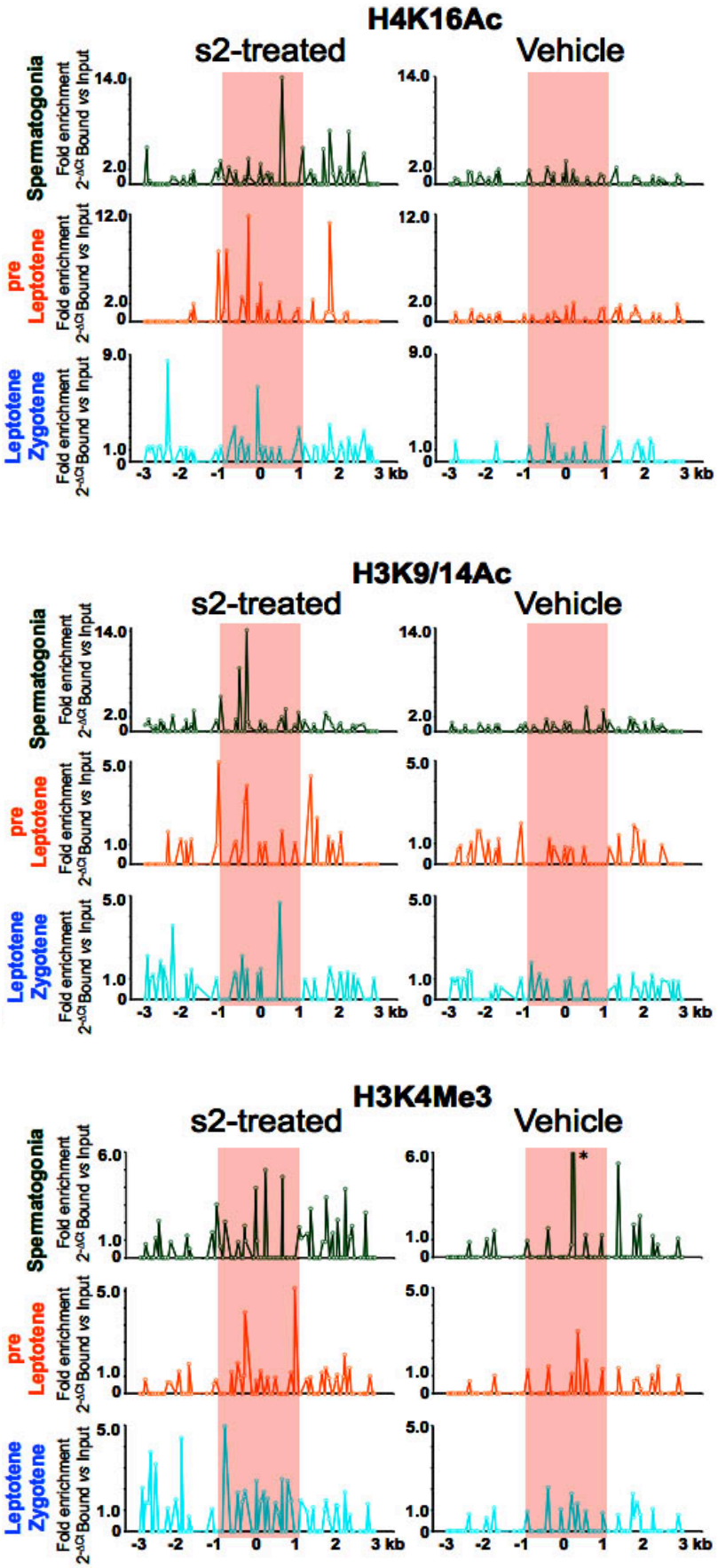

Getun *et al.* Figure S10

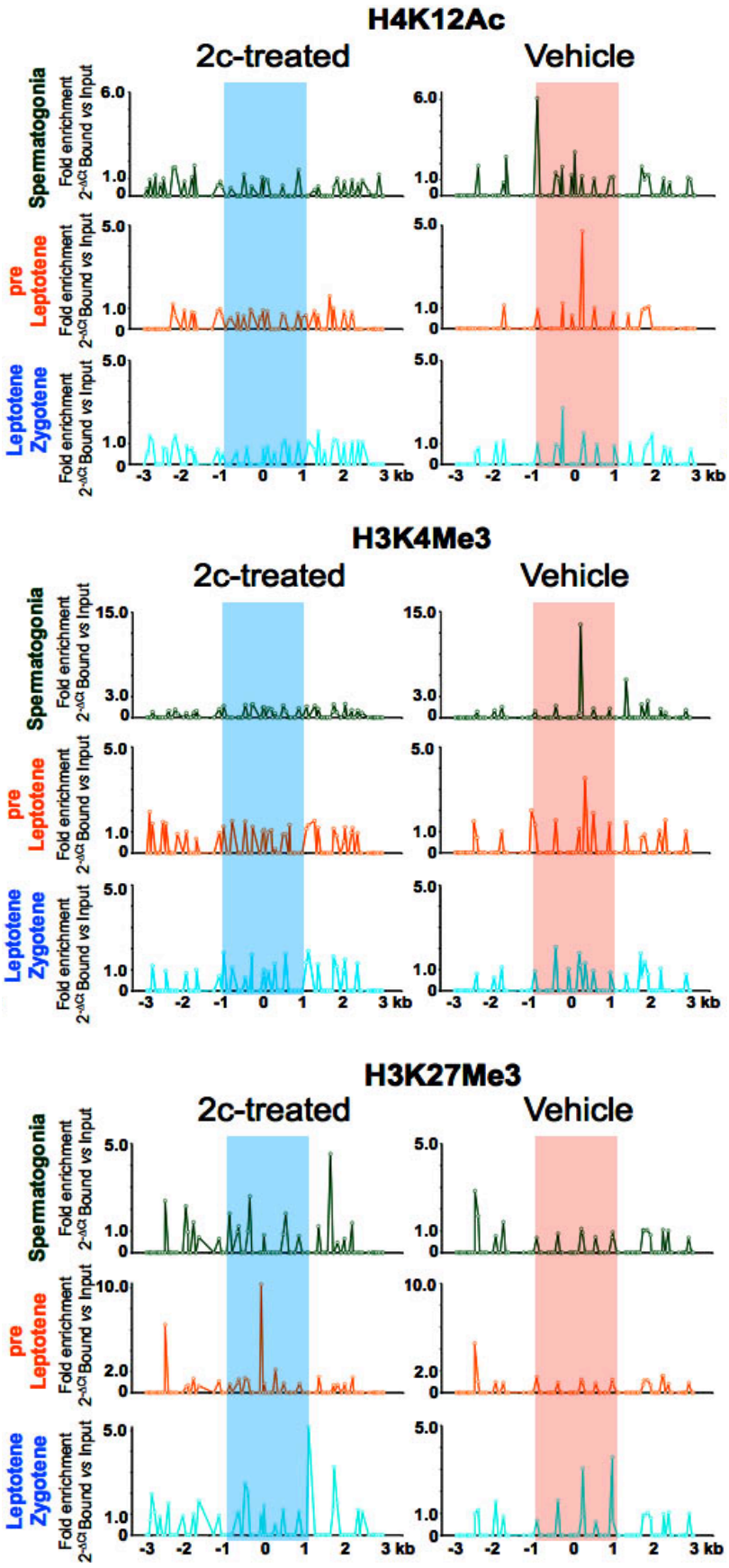

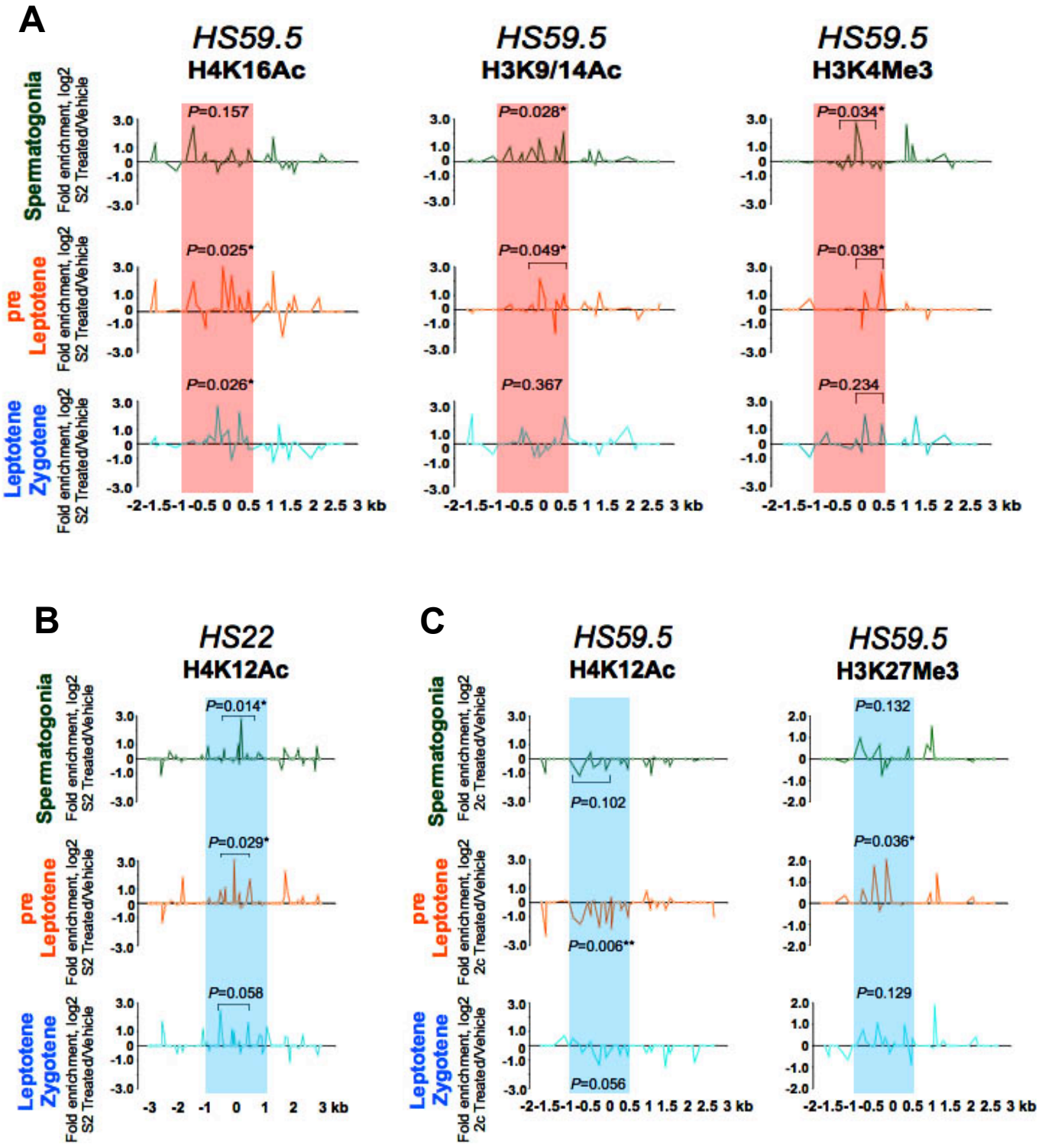
A
HS59.5
H4K16Ac
HS59.5
H3K9/14Ac
HS59.5
H3K4Me3
Spermatogonia
pre Leptotene
Leptotene Zygotene
Fold enrichment, log2 S2 Treated/Vehicle
P=0.157
P=0.025*
P=0.026*
P=0.028*
P=0.049*
P=0.367
P=0.034*
P=0.038*
P=0.234
-2 -1.5 -1 -0.5 0 0.5 1 1.5 2 2.5 3 kb
B
HS22
H4K12Ac
P=0.014*
P=0.029*
P=0.058
-3 -2 -1 0 1 2 3 kb
C
HS59.5
H4K12Ac
HS59.5
H3K27Me3
Fold enrichment, log2 2c Treated/Vehicle
P=0.102
P=0.006**
P=0.056
P=0.132
P=0.036*
P=0.129

A

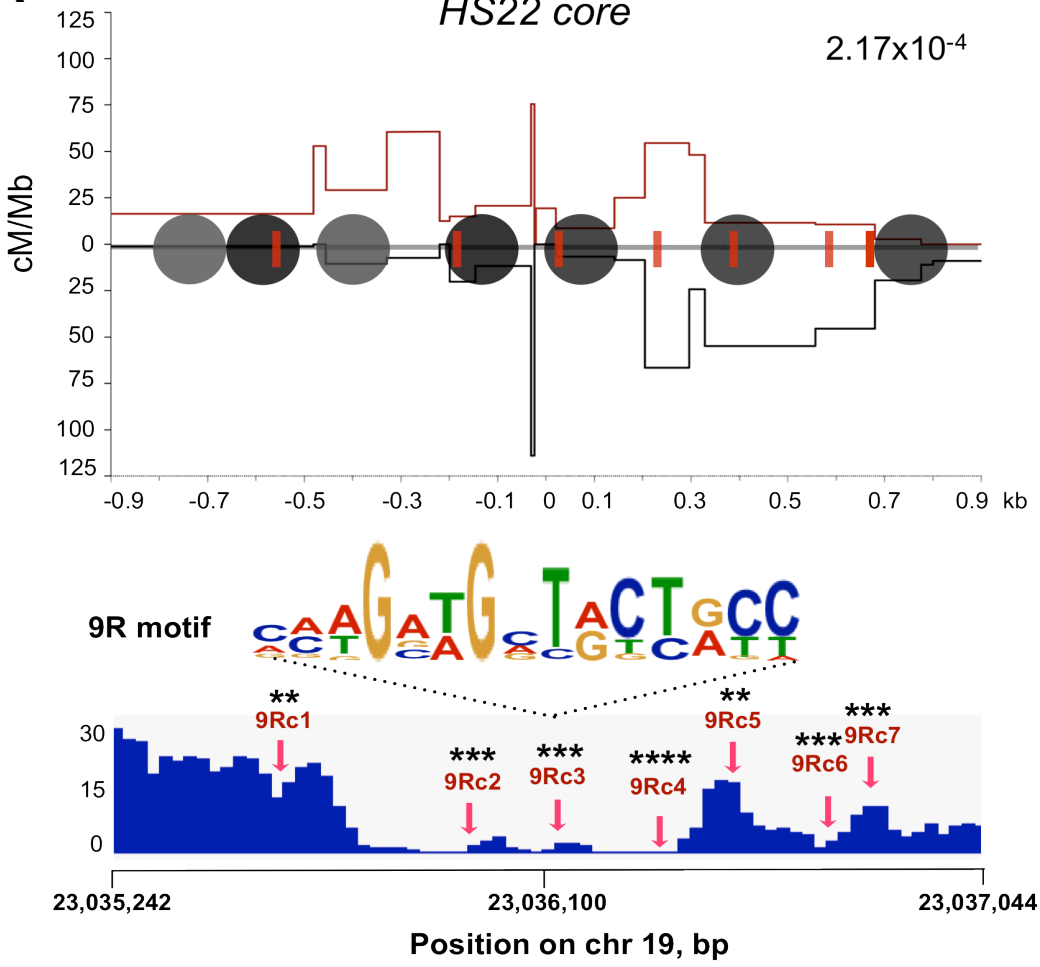
HS22 core
2.17x10-4
cM/Mb
125
100
75
50
25
0
25
50
75
100
125
-0.9
-0.7
-0.5
-0.3
-0.1
0
0.1
0.3
0.5
0.7
0.9
kb
9R motif
**
9Rc1
***
9Rc2
***
9Rc3
****
9Rc4
**
9Rc5
***
9Rc6
***
9Rc7
30
15
0
23,035,242
23,036,100
23,037,044
Position on chr 19, bp

B

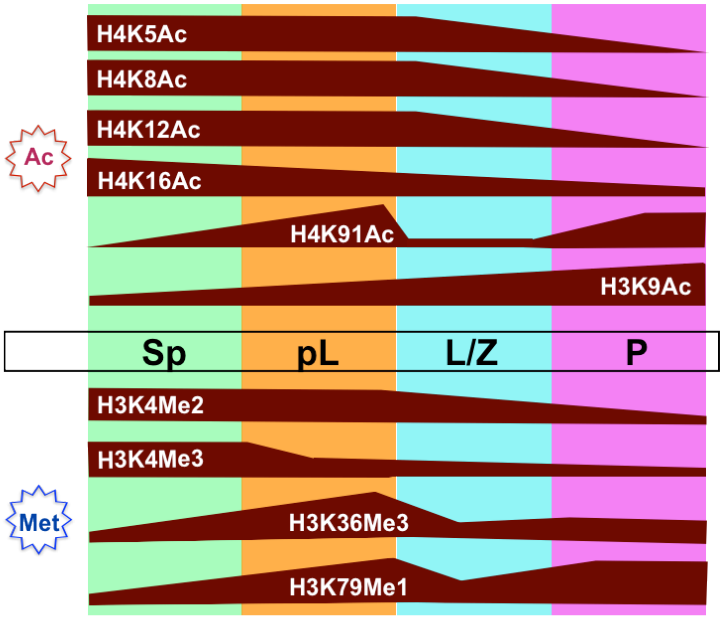
H4K5Ac
H4K8Ac
H4K12Ac
H4K16Ac
Ac
H4K91Ac
H3K9Ac
Sp
pL
L/Z
P
H3K4Me2
H3K4Me3
Met
H3K36Me3
H3K79Me1

HS22 core